RSC Advances

ROYAL SOCIETY OF CHEMISTRY

www.rsc.org/advances

Journal Name

ARTICLE

Facile fabrication of 3D SnO₂/Nitrogen-doped graphene aerogels for superior lithium storage

Xia Hong, Junfei Liang,* Hua Fan and Lin Guo*

A facile approach to synthesize 3D SnO₂/Nitrogen-doped graphene aerogels (SNGA) was developed. By using ethylenediamine (EDA) as nitrogen source, combined with hydrothermal-induced reduction and self-assembly, the reduction of graphene oxide (GO) to graphene, the uniform in situ deposition of SnO₂ nano-particles on graphene, the Nitrogen-doping of graphene, and the self-assembly of graphene to 3D aerogels were realized in one step. The as-prepared SNGA exhibited a high reversible specific capacity of 986 mA h g⁻¹ at a current density of 100 mA g⁻¹ after 100 cycles and excellent rate capability at different current density. Furthermore, a reversible capacity as high as 508 mA h g⁻¹ was still achieved after 500 cycles even at a high current density of 1 A g⁻¹. The electrochemical test results show that the SNGA prepared by the one-pot method are outstanding anode materials for lithium-ion batteries (LIBs). The superior electrochemical performance of the SNGA is primarily ascribed to its specific structure. The method presented in this paper may provide an effective, economic and green strategy for the preparation of other metal-oxide/Nitrogen-doped graphene aerogels for various applications.

Introduction

Modern electronic devices such as mobile communication devices, portable electronic devices and electric/hybrid vehicles require high-performance batteries to power them. LIBs is one of the most suitable candidates to satisfy the requirements because of their high energy density, high working voltage, and light weight.[1] In the case of a battery, electrode material is a determining factor for the battery performance.[2] Although graphite performs well as anode for commercial LIBs, its theoretical capacity (372 mA h g⁻¹) is insufficient to satisfy the increasing demand for batteries with higher capacity. For the purpose of improving the energy density of LIBs, scientists have made great efforts to explore alternative anode materials with higher capacity. Many materials including metal oxide, metal sulfide, and nonmetal with large specific capacity have been studied to replace graphite.[1, 2b, 3] Among these materials, transition metal oxides (MO$_X$, M: Sn, Fe, Co, Cu, etc.) with high theoretical capacities (>600 mAh g⁻¹), have been exploited as anode materials for high performance LIBs since 1980s.[4] Among various MO$_X$, SnO₂ has attracted much attention because of its high theoretical reversible Li⁺ storage capacity (calculated to be 782 mA h g⁻¹), low charge–discharge potential, low cost, natural abundance, and environmental benignity.[5] However, the practical application of SnO₂ and other MO$_x$ as anode is hampered by their poor cycle performance, resulting from poor electronic conductivity, aggregation of metal clusters and severe volume change during the insertion and extraction processes of Li⁺.[6] To address these problems, various methods have been tested.[7] Results have shown that hybridizing MO$_x$ with carbon materials is an effective method to improve the

electronic conductivity and accommodate the strain of volume change of MO$_x$ anode during the lithiation/delithiation process.[8]

Graphene, a one-atom thick and two-dimensional closely packed honeycomb lattice, has received numerous investigations from both the experimental and theoretical scientific communities since the experimental observation of single layer by K. S. Novoselov and A. K. Geim in 2004.[9] Graphene exhibits a number of intriguing properties, such as excellent intrinsic carrier mobility,[10] quantum electronic transport,[11] high mechanical strength and elasticity,[12] superior thermal conductivity,[13] chemical stability within a wide range of electrochemical potentials, and so on.[14] Those excellent properties of graphene make it suitable for fabrication into high-performance composites with other MO$_X$ anode materials for LIBs. Up to date, by using chemistry solution processes, a lot of papers related to the preparation of SnO₂/graphene nanocomposites with improved Li-storage performance at lower charge/discharge current densities have been reported.[15] However, in most cases of the reported SnO₂/graphene nanocomposites, a serious problem is that the graphene nanosheets would easily reaggregate during the preparation process due to the strong van der Waals forces between graphene sheets. The reaggregation of graphene leads to slow electron and ion transfer and reduce the accessible surface area of graphene sheets, these two factors are not beneficial to enhance the lithium storage performance of the nanocomposites at higher charge/discharge current densities. One strategy to overcome this issue is to assemble graphene sheets into 3D architectures. By forming the 3D network microstructure, the reaggregation and restack problem of graphene sheets during the preparation process could be minimized or prevented. As a group of novel porous materials with advantages of continuous

porosity, high surface area, fast electron and ion transport kinetics, 3D oxide–graphene xerogels can be explored as novel electrode materials with super lithium storage performance.[16]

It is noteworthy, on the other hand, recent research showed the lithium storage properties of graphene can be obviously improved by doping of nitrogen atoms into the graphene lattice. The unique two-dimensional structure, disordered surface morphology, heteroatomic defects, better electrode/electrolyte wettability, increased intersheet distance, improved electrical conductivity, and thermal stability of the Nitrogen-doped (N-doped) graphene are beneficial to rapid surface Li^+ absorption and ultrafast Li^+ diffusion and electron transport, and thus make the N-doped graphene superior to those of pristine chemically derived graphene.[17]

On the basis of so many extraordinary properties of 3D oxide–graphene xerogels and N-doped graphene mentioned above, we expected to see that the SNGA may become an excellent electrode material for the LIBs. However, to date, reports in this topic are very rare. Furthermore, to our best knowledge, there have been no reports concerning the direct preparation of SNGA by a simple route.

Herein, we developed a facile one-step hydrothermal route to chemically synthetize SNGA from GO, EDA and Sn^{4+} for the first time. The advantages of this work are characterized by a facile and green one-step procedure, that is, the reduction of GO to graphene, the uniform in situ deposition of SnO_2 nanoparticles on graphene, the Nitrogen-doping of graphene, and the self-assembly of graphene to 3D aerogels occur simultaneously under mild conditions. In our procedure, rigorous conditions or special instruments, the toxicity of the precursors are not required for the doping of graphene; an extra reducing agent such as toxic hydrazine or sodium borohydride is not required for the reduction of GO to graphene. Furthermore, excellent lithium storage performance of the as-synthesized SNGA as anode material for LIBs was also obtained.

Experimental section

Chemical reagents and materials: Graphite powder (325 mesh, with purity >99.99%) was obtained from Alfa Aesar. All other chemicals (purchased from Aladdin-Reagent Inc.) used in this experiment were analytical grade and were used without further purification.

Preparation of SNGA: GO was synthesized from natural graphite powder by the modified Hummer's method.[18] Then, the GO was subjected to dialysis for 7 days to completely remove metal ions and acids. In order to obtain GO nanosheets dispersed in water, the solution after dialysis was ultrasonicated for 2 h with a frequency of 40 kHz (KH-500, Kunshan, Hechuang Ultrasonic Cleaner Inc.). Subsequently, the suspension of GO nanosheets was treated by high-speed centrifugation (10000 rpm, 20 min) to remove any undispersed solid, and afterwards, a brown homogeneous supernatant was collected.

In a typical synthesis of the SNGA, 0.5 g of $SnCl_4 \cdot 5H_2O$ was added to the resulting homogeneous dispersion of GO (20 ml, 2 mg/ml). The mixture was stirred for 5 min before adding 0.5 mL of EDA. Then the mixture was stirred at ambient conditions for another 5 min. The resulting solution was transferred to a Teflon-lined stainless steel autoclave of 25 mL volume and kept at 180 ℃ for 24 h, leading to phase separation in the autoclave, with a black SnO_2/Nitrogen-doped graphene hydrogel (SNGH) forming. The SNGH was taken out, washed with distilled water, and freeze-dried, leading to formation of the SNGA.

Characterizations: The structures and compositions of the as-prepared products were characterized by X-ray powder diffraction (XRD) using a Rigaku Dmax 2200 X-ray diffractometer with Cu Kα radiation (λ= 1.5416 Å). The XRD specimens were prepared by means of flattening a piece of SNGA on the small slides. Transmission electron microscopy (TEM) and high-resolution TEM (HRTEM) investigations were carried out by a JEOL JEM-2100F microscope. The as-prepared samples were dispersed in ethanol and dropped onto a carbon film supported on a copper grid for the drying process in air. Raman spectrometer was recorded on a LabRAM HR800 (HORIBA Jobin Yvon) confocal Raman spectrometer, with an excitation laser wavelength of 488.5 nm. All samples were deposited on silicon wafers in powder form without using any solvent. The XPS data were taken on an AXIS Ultra instrument from Kratos Analytical. The IR spectra were carried out through a Nicolet iN10 MX (Thermo Scientific) in the infrared domain 600～4000 cm^{-1}.

Electrochemical measurements: The electrochemical properties of the SNGA nanocomposites as anode materials for LIBs were evaluated by galvanostatic charge/discharge technique. The test electrodes were prepared by mixing 80 wt % active material with 10 wt % carbon black and 10 wt % polyvinylidene fluoride (PVDF) dissolved in N-methyl-2-pyrrolidone (NMP) to form a slurry, which was then coated onto a copper foil (current collector), dried at 80 °C for 12 h. Afterwards, CR2032 type coin cells were assembled in an highly-pure argon-filled glovebox using the test electrodes, the metallic lithium counter/reference electrode, a separator (Whatman, GF/D), an electrolyte of 1 mol/L LiPF6 in ethylene carbonate and diethyl carbonate (EC/DMC, 1:1 vol) (Tianjin Jinniu Power Sources Material Co., Ltd. China). Charge-discharge measurements were carried out galvanostatically at different current density in the voltage range of 0.005 V ～ 3 V using a battery test system (LAND CT2001A model, Wuhan Jinnuo Electronics. Ltd., China).

Results and discussion

In this work, we developed a convenient hydrothermal method to fabricate SNGA. The overall procedure is illustrated in Scheme 1. Previous studies have indicated that the GO nanosheets have their basal planes decorated mostly with epoxy and hydroxyl groups, in addition to carboxyl groups located presumably at the edges.[19] First, the GO was dispersed in H_2O to form a uniform GO nanosheets suspension with the aid of sonication because of the oxygen-containing species. When GO solution was mixed with $SnCl_4 \cdot 5H_2O$, the Sn^{4+} was selectively
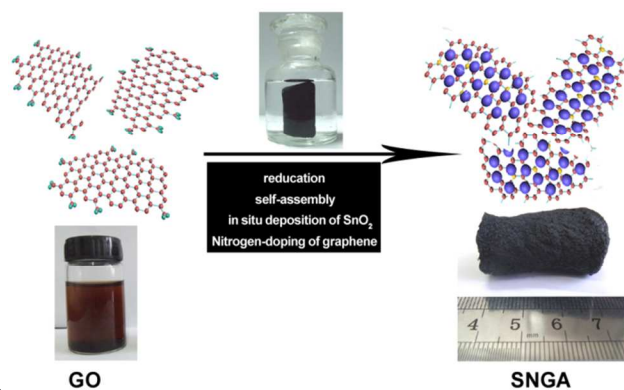
Scheme 1 Schematic illustration of fabrication of SNGA.

bonded with the oxygenated groups by electrostatic force.[20] After reacted at 180 °C for 24h, the GO sheets were reduced to graphene sheets and the graphene sheets were self-assembled to form the 3D architectures. The SnO_2 nanoparticles could nucleate and simultaneously grow in situ on the graphene surface during this process. Our process can ensure the in situ formation of SnO_2 nanoparticles uniformly and the self-assembly of graphene to 3D architectures simultaneously, with the advantages of alleviating any serious restacking of graphene sheets and preventing the agglomeration of SnO_2 nanoparticles. Meanwhile, because of the presence of EDA as the nitrogen source, the N-doping of graphene can occur simultaneously under the hydrothermal condition. After the hydrothermal reaction, phase separation took place in the reaction vessel: the SNGH were formed (except for the integrated cylinder, there were no separated graphene sheets elsewhere. Finally, a 3D monolithic architecture of black SNGA was obtained by freeze-drying the SNGH.

The morphology and structure of the SNGA were studied using SEM and TEM. As summarized in Fig. 1a and 1b, the as-prepared SNGA exhibited well-defined and interconnected 3D microstructures, with uniformly dispersed micron-sized pores. The walls of the 3D microstructures consisting of graphene sheets were rather thin, indicating the effective assembly of graphene sheets. Fig. 1c shows a low magnification TEM image of the SNGA, worm-like SnO_2 nanoparticles are uniformly distributed on the surface of ultrathin graphene sheets. A HRTEM image of the SNGA is shown in Fig. 1d, showing the average particle size of the SnO_2 is less than 6 nm. The lattice-resolved image of SNGA shows a lattice spacing of 0.33 nm, which is corresponding to the d-spacing of (110) crystal planes of SnO_2. The strips marked with arrows in Fig. 1d shows the exiting of graphene nanosheets in the SNGA. The successful in situ deposition of uniformly-dispersed small size SnO_2 nanocrystallites on graphene sheets can be realized because of the existence of GO and EDA in the reaction system. The abundant oxygenated functional groups (epoxy-, hydroxyl-, carboxyl-), presumed to be uniformly distributed on the surface of the GO sheets,[19] can act as anchoring sites for Sn^{4+} through

electrostatic attraction.[20] Those oxygenated groups coordinated with the Sn^{4+} can further act as the nucleation center for the SnO_2 nanoparticles growth. This process could ensure the in situ deposition of a uniformly nanoparticle on graphene, with the advantage of preventing the agglomeration of SnO_2 nanoparticles.[21] In addition to that, after N-doping, the graphene can provide more active and nucleation sites, which facilitate the morphology and particle size control of the SNGA. Moreover, some research demonstrates that GO can play an important role in the morphology and size control of the resultant particles during the particle growth process due to its surfactant effect. The uniform and small size of particles can be obtained from the GO involved systems.[22] On the other hand, the formation of SnO_2 can be attributed to the hydrolysis reaction of Sn^{4+}. In our work, EDA plays the role of ligand, it was thought that the existence of the EDA in the reaction system decreased the hydrolysis reactivity between Sn^{4+} and OH group because of the strong coordination between Sn^{4+} and EDA, and resulted in the formation of small size SnO_2 nanocrystallites. Our method was expected to improve LIBs properties due to the very small particle size of SnO_2. Because the small particle size can not only endow the composite electrode materials a superior high surface area to buffer the serious volume expansion/contraction of the SnO_2 during the charge/discharge processes but also shorten the diffusion distance for Li^+ and bring the satisfied conductivity to single SnO_2 nano-particles.

The representative XRD pattern of GO and SNGA are shown in Fig. 2a. The peak at 10.4° in curve a is characteristic for GO with an interlayer spacing of 0.85 nm. For samples of SNGA, no diffraction peaks of layered GO can be observed, indicating the successful reduction of GO.[23] No diffraction peak (002) of graphite around 26.6° is observed in the XRD pattern of the SNGA, which demonstrates the absence of layer-stacking regularity after the reduction of GO, because the graphene sheets were efficiently assembled together into the 3D network microstructure. By forming the 3D network microstructure, the reaggregation and restack problem of graphene sheets during the reduction process could be minimized or prevented, favoring the maintenance of high surface area and other intrinsic chemical and physical properties of graphene, which is
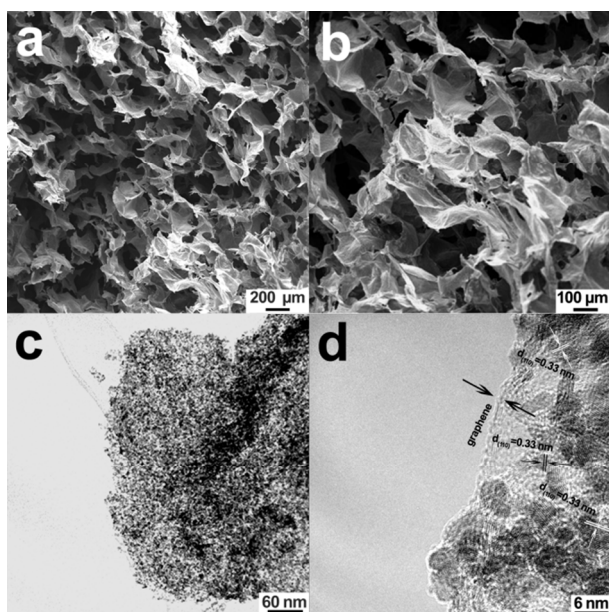

Fig. 1 SEM images of SNGA (a) at low magnification, and (b) at high magnification; TEM images of SNGA (c) at low magnification, and (d) at high magnification.
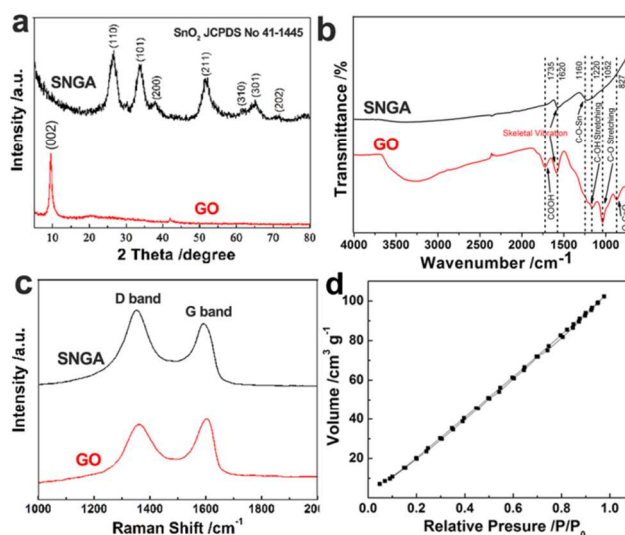

Fig. 2 (a) XRD patterns; (b) FT-IR spectra and (c) Raman spectra of GO and the SNGA; (d) N_2 adsorption-desorption isotherms of the SNGA.

beneficial for improving the Li$^+$ storage performance of the SNGA. The XRD pattern of SNGA matchs well with standard SnO_2 card (JCPDS no. 41-1445), suggesting the successful complexation of SnO_2 into the graphene nanosheets. These diffraction peaks are considerably broadened, indicating the SnO_2 particles are very small in size. IR spectrum of GO (Fig. 2b) shows the O-H deformation peak at 1401 cm^{-1}, a weak band at 1735 cm^{-1} assigned to COOH, 1220 cm^{-1} assigned to C-OH stretching, 1052 cm^{-1} due to C-O stretching vibrations, and 827 cm^{-1} due to (O-C=O). Both spectra depict a peak at 1620 cm^{-1} which corresponds to the remaining sp^2 character.[15b] Most of oxygen-containing groups of GO are removed after the hydrothermal reaction, which can be seen from the IR spectrum of SNGA. It is well known that the hydrothermal reduction of GO is a very important method to prepare graphene.[24] Moreover, the amines of EDA can react with the oxygen-containing moieties to reduce GO.[25] The IR results further confirm the reduction of GO to graphene. Raman spectroscopy is a powerful tool to characterize carbonaceous materials. Fig. 2c shows the Raman spectra of GO and SNGA, which clearly reflect significant structural changes during the process from GO to SNGA. The Raman spectra of GO and SNGA both contain G band (E$_{2g}$ phonon of C sp^2 atoms) and D band (κ-point phonons of A$_{1g}$ symmetry); however, compared with GO, the D/G intensity ratio of SNGA increased obviously. This is a commonly observed phenomenon for chemically converted graphene because the newly formed myriad of sp^2 domains decreased the average size of all the sp^2 domains upon reduction of the GO sheets.[26] This change of Raman spectra from GO to SNGA also indicates the successful reduction of GO and the forming of graphene. N$_2$ adsorption–desorption isotherm of SNGA was measured by Brunauer Emmett Teller (BET) method (Fig. 2d). Specific surface area of the SNGA was obtained to be 112.3 m^2 g^{-1}, which is bigger than the value of reported graphene aerogel.[27] The higher specific surface area can provide more surface reaction sites and is favorable for the electrochemical properties.

The status of the N-doping can be unraveled by the elemental mapping images of C, N in the SNGA. The TEM elemental mapping (Fig. 3a) reveals that the distribution of nitrogen heteroatoms in the plane of graphene is highly homogeneous. The elemental mapping image of Sn further confirms the SnO_2 nanocrystallites are distributed on the graphene uniformly, which is consistent with the TEM observations above. XPS is a powerful tool to identify the elements' states in bulk material. To confirm the N-doping of graphene, XPS studies were carried out. In the SNGA, the N1s peak has three components, indicating that N atoms are in the three different bonding characters inserted into the graphene network (Fig. 3b). The peaks at 399.2 eV and 400.2 eV are attributed to the pyridinic N (N1) and pyrrolic N (N2), respectively.[28] They refer to the N atoms which are located in a π conjugated system and contribute to the π system with one or two p-electrons, respectively.[29] The peak at 401.4 eV corresponds to quaternary N or the "graphitic" N (N3), which refers to the N atoms replacing the C atoms inside of the graphene layers.[30] Fig. 3c shows the C1s XPS patterns of GO and SNGA. In the case of GO sample, the spectrum can be deconvoluted into three components, the main peak centered at about 284.8 eV originated from the graphitic sp^2 carbon atoms, the binding energies located at 286.8 eV and 288.1 eV are due to carbon atoms connecting with oxygenate groups, such as C–OH and O–C=O, respectively. Compared with GO, the oxygenate species is substantially removed with the reduction of GO to
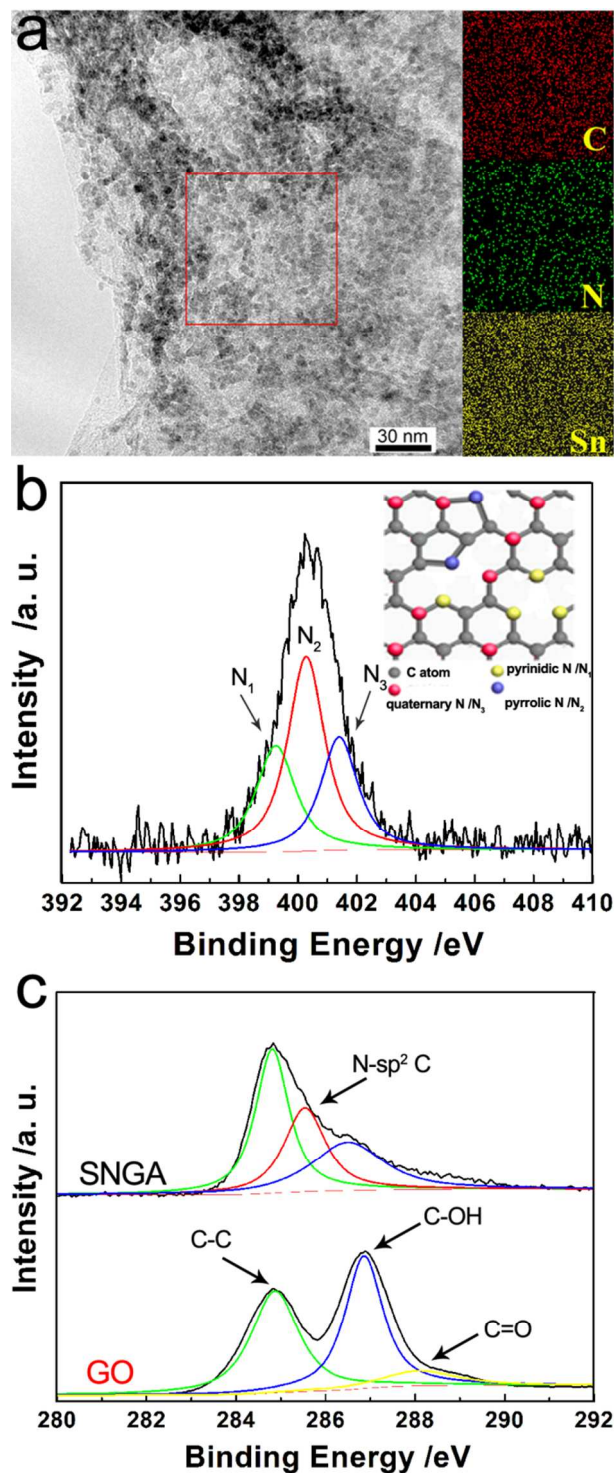

Fig. 3 (a) TEM image obtained from the SNGA and C-, N- and Sn- elemental mapping of the square region; (b) the high-resolution XPS spectra of the N1s region for SNGA, (c) the high-resolution XPS spectra of the C1s region for GO and SNGA.

graphene, which suggests a considerable de-oxygenation process and the successful formation of graphene. A residual weak peak of C-OH can be seen in Fig. 3c, this result is in good agreement with the IR characterization where a weak O-H deformation peak existed. A new peak at 285.5 eV corresponding to the N-sp^2 C appears, which reflects the bonding structure of the C-N bonds and is originated from

substitution of the N atoms, defects or the edge of the graphene sheets.[29b] On the other hand, the XPS patterns of Sn 3d (Fig. S1) further indicates the existence of SnO_2 nanocrystals in the SNGA. On the basis of XPS analysis discussed above, we can conclude that the reduction of GO to graphene, the deposition of SnO_2 nanoparticles on graphene, and the Nitrogen-doping of graphene can be realized in one step by our method. Due to nitrogen has higher electronegativity (3.5) than carbon (3.0), and smaller diameter, the stronger interaction between the formed carbon structure and lithium might be favorable for lithium kinetics. The pyridine and pyrrolic N atoms are satisfactorily bonded and may contribute to an enhancement of reversible capacity.[31]

The 3D architectures, N-doped graphene layers, and highly dispersed small size SnO_2 nanocrystals are desirable features for SNGA electrode materials in LIBs. Fig. 4a shows the typical charge/discharge profiles of the SNGA in the 1st, 20th, and 100th cycles under a current density of 100 mA g^{-1}. The capacity dropped rapidly in the first cycle due to the irreversible formation of amorphous Li_2O matrix and intense surface reactions between the Li−Sn compounds and the electrolyte solution to form a solid electrolyte interface layer (SEI).[15c] In the subsequent charge/discharge cycles, Li^+ were reversibly inserted into Sn as Li_xSn alloys. After the initial capacity fading, the shape of the profiles did not change basically, indicating the good stability of the SNGA as an anode, and even a little increase of the capacity is observed. The cycle performance of the SNGA and the single SnO_2 nanocrystallites are shown in Fig. 4b. The SNGA exhibited a high reversible discharge capacity of 1128.5 mA h g^{-1} at the second cycle, and from the second cycle, it showed better cycle performance and highly reversible behavior. After 100 cycles, the SNGA can keep about 87.4 % retention of the initial reversible capacity, and a discharge capacity of 986.3 mA h g^{-1} still can remain. This performance is better than other reported SnO_2/graphene nanocomposite for LIBs.[15] On the other side, the specific capacity of the SnO_2 nanoparticle electrode rapidly decreased to 163 mAh g^{-1} after 50 cycles, just hold about 24.6% retention of the reversible capacity due to the severe pulverization of the electrode materials. Compared with the single SnO_2 nanoparticles, the SNGA exhibit superior discharge capacity and cycling performance. The rate performance of the SNGA is

shown in Fig. 4c, which was tested at the varied current density from 100 to 2000 mA g^{-1}. The SNGA shows an excellent rate capability. At the higher current densities of 200, 500, and 1000 mA g^{-1}, the SNGA can display specific discharge capacities of 979, 870, and 722 mA h g^{-1}, respectively. Even if the highest current density of 2000 mA g^{-1} was used, the SNGA can still exhibit a high substantial capacity of 509 mA h g^{-1}. It is worth pointing out that, even after 50 cycles, the SNGA still had the ability to display a reversible capacity of 1037 mA h g^{-1} when the current density was reversed back to 100 mA g^{-1}. This result demonstrates that 89% of the initial reversible capacity of the SNGA is recovered. As we know, the long-time cyclic stability of electrodes at a high current density is very important in practical applications of LIBs. To further demonstrate the excellent cyclic stability of SNGA, the electrode was tested at a higher current density of 1000 mA g^{-1} with a larger numbers of cycles (Fig. 4d). Under the current density of 1000 mA g^{-1}, the reversible capacity of the cell can be as high as 508 mA h g^{-1} after 500 cycles, demonstrating an extremely promising stable cycling performance over a prolonged testing period. The result of rate capability and long-time cyclic clearly indicates that the SNGA could tolerate changed charge/discharge current densities, which is a desirable feature for high power LIB application.

In order to verify the good electrochemical performance of SNGA, AC impedance spectra measurements were carried out (Fig. S2). The impedance spectra of the SNGA electrodes were obtained in the 5th discharge cycle. The high-frequency semicircle is attributed to SEI film resistance, and the spectra in the medium frequency include features that are usually semicircular in shape and related to charge transfer resistance. From Fig. S2, we can see that the diameter of the semicircle for the SNGA electrode in the high–medium frequency region is rather small, which indicates that the SNGA possess low contact and charge-transfer resistances. The super performance of SNGA observed in our experiments should be attributed to the unique features of the SNGA. First, the SNGA with the advantages of continuous porosity and high surface area, gives rise to a large contact area between the active material and the electrolyte. Moreover, in the SNGA, the graphene sheets with a high surface area build an excellent 3D conductive network which can promote electron transfer during the lithiation and de-lithiation processes. These two factors are beneficial for improving the capacity of USNG under the higher current density. Second, the main reason for the rapid fading of SnO_2 electrode is that the large volume change of the SnO_2 occurs during the charge−discharge cycle, leading to cracking and pulverization of the electrode. N-doped graphene can still kept the excellent mechanical properties of pristine graphene. A super flexible coating made of high mechanically flexible N-doped graphene sheets covered with the SnO_2 nanocrystals not only provides an elastic buffer space to accommodate the volume changes upon lithium-ion insertion/extraction but also efficiently prevents the aggregation of the nanoparticles and the cracking or crumbling of the electrode material. As a result, a better cycle stability can be obtained. Even though volume expansion still exists, the electrode will not pulverize as the graphene sheets can deform resiliently to accommodate such volume changes.[32] Third, compared with the pristine graphene, the doped nitrogen atoms can provide extra lone pair electrons, and as a result, the electron density of graphene will be augmented, which makes the N-doped graphene shows more excellent electrical conductivity than the pristine graphene.[17a, 33] Therefore, the conductivity of the SNGA can be dramatically
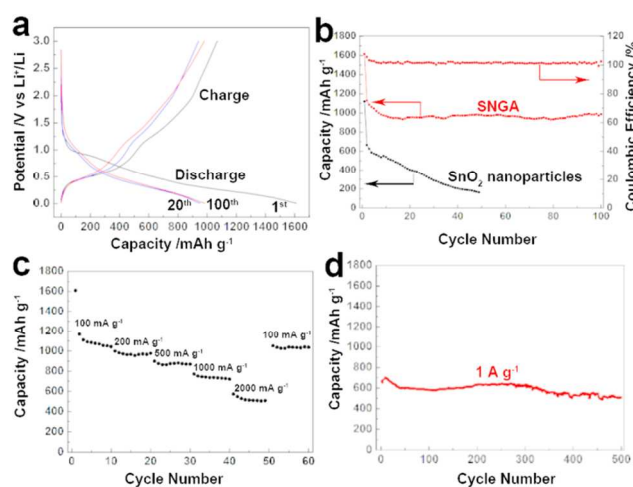

Fig. 4 (a) Charge/discharge profile for SNGA; (b) The cycle performance of SNGA and single SnO_2 nanocrystallites at a current density of 100 mA g^{-1}; (c) Rate performance of the SNGA; (d) The cycle performance of SNGA at a current density of 1000 mA g^{-1}.

enhanced because of the presence of the super electroconductive N-doped graphene. Moreover, the N-doped graphene sheets with high surface area can build a better conductive network which could promote the electron transfer during the lithiation and de-lithiation process. In the SNGA, the electronic transport speed is effectively accelerated compared with the single SnO_2 nanocrystals. Futhermore, the N-doped graphene sheets can provide a continuous conductive path in between the SnO_2 nanocrystals, which can reduce the particle−particle interface resistance effectively. The in situ forming of the SnO_2 nanoparticles, the electrostatic attraction between electron-rich Sn atoms and electron-unsaturated carbon atoms of graphene enable the SnO_2 nanocrystals to be firmly anchored on graphene surface and thus enhance the conjunction stability of the composites. The close contact between the SnO_2 nanoparticles and the super electroconductive N-doped graphene can also minimize the electrical isolation of nanoparticles during battery cycles. Fourthly, by N-doping, a large number of topological defects are induced to the graphene sheet, and a disordered carbon structure with many surface defects is formed, which make the insertion and extraction processes of Li became much easier, leading to the increase of the reversible capacity. Moreover, the reversible capacity of the pristine graphene can be improved by introducing the pyridine and pyrrolic N atoms.[34] Fifthly, the good dispersion of small size SnO_2 nanocrystallites on graphene with large specific surface area can not only give rise to a large contact area between the active material and the electrolyte, but also provide a fast and versatile transport pathways for the electrolyte ions. The above synergetic effects arising from the particular structure of SNGA is responsible for the excellent lithium storage performance of the SNGA electrode.

Conclusions

In summary, a facile one-step hydrothermal route to in situ chemically synthetize SNGA was developed. The advantages of this work are characterized by a facile, low-cost and green one-step procedure. The electrochemical results show the SNGA provide a super Li-storage performance. When considering the plentiful properties of both SnO_2 and N-doped graphene, the SNGA could be promisingly applied in many research fields such as ultracapacitors, biosensor, gas sensor, gas storage and electrochemical analysis in the future. Furthermore, this synthesis method may provide a facile, economic, and green strategy for the preparation of other metal-oxide/N-doped graphene aerogels for different applications.

Acknowledgements

Notes and references

Key Laboratory of Bio-Inspired Smart Interfacial Science and Technology of Ministry of Education, School of Chemistry and Environment, Beihang University, 37 Xueyuan Road, Haidian District, Beijing 100191, China. Fax: +86-10-8233 8162; Tel: +86-10-8233 8162; E-mail: guolin@buaa.edu.cn.

Electronic Supplementary Information (ESI) available: [The XPS patterns of Sn 3d]. See DOI: 10.1039/b000000x/

1 J. M. Tarascon and M. Armand, *Nature*, 2001, **414**, 359.
2 (a) K. S. Kang, Y. S. Meng, J. Breger, C. P. Grey and G. Ceder, *Science,* 2006, **311**, 977; (b) C. K. Chan, H. L. Peng, G. Liu, K. McIlwrath, X. F. Zhang, R. A. Huggins and Y. Cui, *Nat. Nanotechnol. ,* 2008, **3**, 31.
3 A. S. Arico, P. Bruce, B. Scrosati, J. M. Tarascon and W. Van, Schalkwijk, *Nat. Mater.,* 2005, **4**, 366.
4 (a) M. M. Thackeray and J. A. Coetzer, *Mater. Res. Bull.,* 1981, **16,** 59; (b) M. M. Thackeray, W. I. F. David, P. G. Bruce, J. B. Goodenough, *Mater. Res. Bull.,* 1983, **18**, 461.
5 Y. Idota, T. Kubota, A. Matsufuji, Y. Maekawa, T. Miyasaka, *Science*, 1997, **276**, 1395.
6 (a) J. Yang, Y. Takeda, N. Imanishi, O. Yamamoto, *J. Electrochem. Soc.,* 1999, **146**, 4009; (b) D. Larcher, S. Beattie, M. Morcrette, K. Edstroem, J. C. Jumas and J. M. Tarascon, *J. Mater. Chem.,* 2007, **17**, 3759.
7 (a) C. Wang, Y. Zhou, M. Y. Ge, X. B. Xu, Z. L. Zhang and J. Z. Jiang, *J. Am. Chem. Soc.,* 2010, **132**, 46; (b) M. S. Park, G. X. Wang, Y. M. Kang, D. Wexler, S. X. Dou and H. K. Liu, *Angew. Chem., Int. Ed.,* 2007, **46**, 750; (c) H. Wang, Y. M. Wu, Y. S. Bai, W. Zhou, Y. R. An, J. H. Li and L. Guo, *J. Mater. Chem.,* 2011, **21**, 10189; (d) Y. Wang, J. Y. Lee and H. C. Zeng, *Chem. Mater.,* 2005, **17**, 3899.
8 (a) X. W. Lou, J. S. Chen, P. Chen and L. A. Archer, *Chem. Mater.,* 2009, **21**, 2868; (b) X. W. Lou, C. M. Li and L. A. Archer, Adv. Mater., 2009, **21**, 2536; (c) L. Yuan, K. Konstantinov, G. X. Wang, H. K. Liu and S. X. Dou, *J. Power Sources,* 2005, **146**, 180.
9 K. S. Novoselov, A. K. Geim, S. V. Morozov, D. Jiang, Y. Zhang, S. V. Dubonos, I. V. Grigorieva and A. A. Firsov, *Science,* 2004, **306**, 666.
10 K. I. Bolotin, K. J. Sikes, Z. Jiang, M. Klima, G. Fudenberg, J. Hone, P. Kim and H. L. Stormer, *Solid State Commun.,* 2008, **146,** 351.
11 (a) K. S. Novoselov, A. K. Geim, S. V. Morozov, D. Jiang, M. I. Katsnelson, I. V. Grigorieva, S. V. Dubonos and A. A. Firsov, *Nature*, 2005, **438**, 197; (b) Y. Zhang, Y. W. Tan, H. L. Stormer and P. Kim, *Nature*, 2005, **438**, 201.
12 C. Lee, X. Wei, J. W. Kysar and J. Hone, *Science,* 2008, **321**, 385.
13 A. A. Balandin, S. Ghosh, W. Bao, I. Calizo, D. Teweldebrhan, F. Miao and C. N. Lau, *NanoLett.,* 2008, **8**, 902.
14 (a) A. K. Geim, *Science,* 2009, **324**, 1530; (b) H. –P. Cong, X. –C. Ren, P. Wang, S. -H. Yu, *Sci. Rep.,* 2012, **2**, 613.
15 (a) S. M. Paek, E. Yoo and I. Honma, *Nano Lett.,* 2009, **9**, 72; (b) L. S. Zhang, L. Y. Jiang, H. J. Yan, W. D. Wang, W. Wang, W. G. Song, Y. G. Guo and L. J. Wan, *J. Mater. Chem.,* 2010, **20**, 5462; (c) Y. M. Li, X. J. Lv, J. Lu and J. H. Li, *J. Phys. Chem. C,* 2010, **114**, 21770; (d) K. Shiva, H. B. Rajendra, K. S. Subrahmanyam, A. J. Bhattacharyya and C. N. R. Rao, *Chem.–Eur. J.,* 2012, **18**, 4489; (e) J. F. Liang, W. Wei, D. Zhong, Q. L. Yang, L. D. Li and L. Guo, *ACS Appl. Mater. Interfaces,* 2012, **4**, 454; (f) X. F. Li, X. B. Meng, J. Liu, D. S. Geng, Y. Zhang, M. N. Banis, Y. L. Li, J. L. Yang, R. Y. Li, X. L. Sun, M. Cai and M. W. Verbrugge, *Adv. Funct. Mater.,* 2012, **22**, 1647; (g) S. J. Ding, D. Y. Luan, F. Y. C. Boey, J. S. Chen and X. W. Lou, *Chem. Commun.,* 2011, **47,** 7155; (h) X. S. Zhou, Y. X. Yin, L. J. Wan and Y. G. Guo, *J. Mater. Chem.,* 2012, **22**, 17456.
16 (a) W. Wei, S. B. Yang, H. X. Zhou, I. Lieberwirth, X. L. Feng and K. Müllen, *Adv. Mater.,* 2013, **22**, 2909; (b) J. Luo, J. Liu, Z. Zeng, C. F. Ng, L. Ma, H. Zhang, J. Lin, Z. Shen and H. J. Fan, *Nano Lett.,* 2013, **13**, 6136; (c) W. F. Chen, S. R. Li, C. H. Chen and L. F. Yan, *Adv. Mater.,* 2011, **23**, 5679; (d) H. P. Cong, X. C. Ren, P. Wang and S. H. Yu, *ACS Nano,* 2012, **6**, 2693; (e) Y. J. Gong, S. B. Yang, Z. Liu, L. L. Ma, R. Vajtai, P. M. Ajayan, *Adv. Mater.,* 2013, **25**, 3979.
17 (a) Z. –S. Wu, W. L. Ren, L. Xu, F. Li, H. –M. Cheng, ACS Nano, 2011, 5, 5463; (b) X. Li, D. Geng, Y. Zhang, X. Meng, R. Li and X. Sun, *Electrochem. Commun.*, 2011, **13**, 822, (c) H. Wang, C. Zhang, Z. Liu, L. Wang, P. Han, H. Xu, K. Zhang, S. Dong, J. Yao and G. Cui, *J. Mater. Chem.,* 2011, **21**, 5430.
18 N. I. Kovtyukhova, P. J. Ollivier, B. R. Martin, T. E. Mallouk, S. A. Chizhik, E. V. Buzaneva and A. D. Gorchinskiy, *Chem. Mater.,* 1999, **11**, 771.
19 S. Stankovich, D. A. Dikin, G. H. B. Dommett, K. M. Kohlhaas, E. Z. Zimney, E. A. Stach, R. D. Piner, S. T. Nguyen and R. S. Ruoff, *Nature,* 2006, **442**, 282.
20 L. S. Zhong, J. S. Hu, Z. M. Cui, L. J. Wan and W. G. Song, *Chem. Mater.,* 2007, **19**, 4557.
21 C. Peng, B. Chen, Y. Qin, S. Yang, C. Li, Y. Zuo, S. Liu and J. Yang. *ACS Nano,* 2012, **6**, 1074.
22 M. S. Zhu, P. L. Chen and M. H. Liu. *ACS Nano,* 2011, **5**, 4529.
23 G. X. Wang, J. Yang, J. Park, X. L. Gou, B. Wang, H. Liu and J. J. Yao. *J. Phys. Chem. C,* 2008, **112**, 8192.

24   Y. Zhou, Q. L. Bao, L. A. L. Tang, Y. L. Zhong, K. P. Loh, *Chem. Mater.,* 2009, **21**, 2950; (b) Y. Xu, K. Sheng, C. Li and G. Shi. *ACS Nano*, 2010, **4**, 4324.

25   P. Chen, J. –J. Yang, S. -S. Li, Z. Wang, T. –Y. Xiao, Y. –H. Qian, S. –H. Yu. *Nano Energy,* 2013, **2**, 249.

26   S. Stankovich, D. A. Dikin, R. D. Piner, K. A. Kohlhaas, A. Kleinhammes, Y. Jia, Y. Wu, S. T. Nguyen and R. S. Ruoff, *Carbon,* 2007, **45**, 1558.

27   (a) H. D. Pham, V. H. Pham, T. V. Cuong, T. D. Nguyen-Phan, J. S. Chung, E. W. Shin and S. Kim, *Chem. Commun.,* 2011, **47,** 9672; (b) X. Zhang, Z. Sui, B. Xu, S. Yue, Y. Luo, W. Zhan and B. Liu, *J. Mater. Chem.,* 2011, **21,** 6494; (c) Z. –S. Wu, S. Yang, Y. Sun, K. Parvez, X. Feng and K. Müllen, *J. Am. Chem. Soc.,* 2012, **134,** 9082; (d) W. Chen, S. Li, C. Chen and L. Yan, *Adv. Mater.,* 2011, **23,** 5679.

28   (a) R. J. J. Jansen and H. Vanbekkum. *Carbon,* 1995, **33**, 1021; (b) Y. Wang, Y. Y. Shao, D. W. Matson, J. H. Li and Y. H. Lin. *ACS Nano,* 2010, **4**, 1790.

29   (a) X. B. Wang, Y. Q. Liu, D. B. Zhu, L. Zhang, H. Z. Ma, N. Yao and B. L. Zhang. *J. Phys. Chem. B*, 2002, **106**, 2186; (b) D. Wei, Y. Liu, Y. Wang, H. Zhang, L. Huang and G. Yu. *Nano Lett.,* 9, **2009**, 1752.

30   J. Casanovas, J. M. Ricart, J. Rubio, F. Illas, J. M. Jimenez-Mateos. *J. Am. Chem. Soc.,* 1996, **118**, 8071.

31   X. C. Ma and E. G. Wang. *Appl. Phys. Lett.,* 2001, **78**, 978.

32   X. Wang, X. Q. Cao, L. Bourgeois, H. Guan, S. M. Chen, Y. T. Zhong, D. M. Tang, H. Q. Li, T. Y. Zhai, L. Li, Y. Bando and D. Golberg. *Adv. Funct. Mater.,* 2012, **22**, 2682.

33   M. Du, C. Xu, J. Sun and L. Gao. *Electrochimica Acta,* 2012, **80**, 302.

34   J. R. Dahn, T. Zheng, Y. Liu and J. S. Xue. *Science*, 1995, **270**, 590.

Table of Content
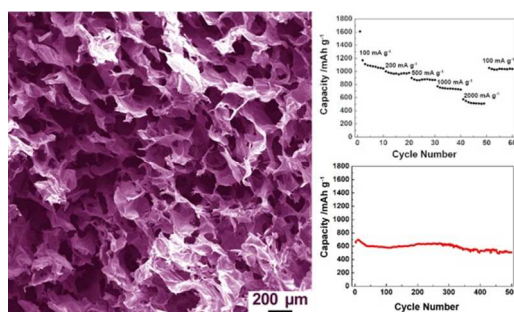
3D SnO2/Nitrogen-doped graphene aerogels was prepared by a facile approach, and demonstrated to have outstanding lithium storage performance